

Reconstructing Cosmological Matter Perturbations using Standard Candles and Rulers

Ujjaini Alam

ISR-1, ISR Division, Los Alamos National Laboratory, Los Alamos, NM 87545, USA

ujjaini@lanl.gov

Varun Sahni

Inter-University Centre for Astronomy and Astrophysics, Pune 411 007, India

varun@iucaa.ernet.in

Alexei A. Starobinsky

Landau Institute for Theoretical Physics, Moscow 119334, Russia ;
RESCEU, Graduate School of Science, The University of Tokyo, Tokyo 113-0033, Japan

alstar@landau.ac.ru

Received _____; accepted _____

ABSTRACT

For a large class of dark energy (DE) models, for which the effective gravitational constant is a constant and there is no direct exchange of energy between DE and dark matter (DM), knowledge of the expansion history suffices to reconstruct the growth factor of linearized density perturbations in the non-relativistic matter component on scales much smaller than the Hubble distance. In this paper we develop a non-parametric method for extracting information about the perturbative growth factor from data pertaining to the luminosity or angular size distances. A comparison of the reconstructed density contrast with observations of large scale structure and gravitational lensing can help distinguish DE models such as the cosmological constant and quintessence from models based on modified gravity theories as well as models in which DE and DM are either unified, or interact directly. We show that for current SNe data, the linear growth factor at $z = 0.3$ can be constrained to 5%, and the linear growth rate to 6%. With future SNe data, such as expected from the JDEM mission, we may be able to constrain the growth factor to 2 – 3% and the growth rate to 3 – 4% at $z = 0.3$ with this unbiased, model-independent reconstruction method. For future BAO data which would deliver measurements of both the angular diameter distance and Hubble parameter, it should be possible to constrain the growth factor at $z = 2.5$ to 9%. These constraints grow tighter with the errors on the datasets. With a large quantity of data expected in the next few years, this method can emerge as a competitive tool for distinguishing between different models of dark energy.

Subject headings: cosmology: cosmological parameters — cosmology: distance scale
— cosmology: theory

1. Introduction

Over the last decade, observations of Type Ia supernovae have shown that the expansion of the universe is currently accelerating (Perlmutter *et al.* 1998; Riess *et al.* 1998; Perlmutter *et al.* 1999; Tonry *et al.* 2003; Riess *et al.* 2005; Astier *et al.* 2005; Riess *et al.* 2007; Wood-Vasey *et al.* 2007; Kowalski 2008). This remarkable discovery has led cosmologists to hypothesize the presence of dark energy (DE), a negative pressure energy component which dominates the energy content of the universe at present. Many theories have been propounded to explain this phenomenon, the simplest of which is the cosmological constant Λ , with a constant energy density and the equation of state $w = -1$. Although Λ appears to explain all current observations satisfactorily, to do so its value must necessarily be very small $\Lambda/8\pi G \simeq 10^{-47}\text{GeV}^4$. So, it represents a new small constant of nature in addition to those known from elementary particle physics, many of them being very small if expressed in the Planck units. However, since it is not known at present how to derive Λ from these small constants and it is also unclear if DE is in fact time independent, other phenomenological explanations for cosmic acceleration have been suggested (see reviews Sahni & Starobinsky 2000; Carroll 2001; Peebles & Ratra 2003; Padmanabhan 2003; Copeland *et al.* 2006; Nojiri & Odinstov 2007; Sahni & Starobinsky 2006). These are based either on the introduction of new physical fields (quintessence models, Chaplygin gas, etc.), or on modifying the laws of gravity and therefore the geometry of the universe (scalar-tensor gravity, $f(R)$ gravity, higher dimensional ‘Braneworld’ models e.t.c.). The plethora of competing dark energy models has led to the development of parametric and non-parametric methods as a means of obtaining model independent information about the nature of dark energy directly from observations (see Starobinsky 1998; Huterer & Starkman 1999; Corasaniti *et al.* 2003; Huterer & Starkman 2003; Alam *et al.* 2004; Saini *et al.* 2004; Jassal *et al.* 2005; Wang & Mukherjee 2006; Lazkoz *et al.* 2006; Alam *et al.* 2007; Sarkar *et al.* 2008; Sahni *et al.* 2008; Sahni & Starobinsky 2006, and references therein).

The next decade will see the emergence of many new cosmological probes. A large number of these are likely to make important contributions to the field of dark energy. The Sloan Digital Sky Survey began its stage III observations in 2008, and its Baryon Oscillation Spectroscopic Survey (BOSS) is expected to map the spatial distribution of luminous galaxies and quasars and detect the characteristic scale imprinted by baryon acoustic oscillations in the early universe (SDSS collaboration). The Joint Dark Energy Mission (JDEM) is expected to discover a large number of supernovae, and also provide important data on weak-lensing and baryon acoustic oscillations (JDEM collaboration). The Square Kilometer Array (SKA) will map out over a billion galaxies to redshift of about 1.5, and is expected to determine the power spectrum of dark matter fluctuations as well as its growth as a function of cosmic epoch (Blake 2004). Important clues to the growth of structure will also come from current and future weak lensing surveys (CFHTLS, DES, JDEM, EUCLID, SKA, LSST), galaxy redshift-space distortions (Guzzo 2008; Song 2008; Percival 2008) as well as galaxy cluster mass functions at different redshifts z (Vikhlinin 2008; Rapetti 2008). With the wealth of data expected to arrive over the next several years, it is important to explore different methods of analyzing these datasets in order to extract the optimum amount of information from them. In this paper we explore the possibility of reconstructing the linearized growth rate of density perturbations in the non-relativistic matter component, $\delta(z)$, taken at some fixed comoving scale much less than the Hubble distance, from datasets which have traditionally been used to explore only the smooth background universe, e.g. luminosity distance and angular diameter distance data.

In the case of *physical* DE, the effective gravitational constant appearing in the equation for linear density perturbations in the matter component coincides with the Newton gravitational constant G measured in the laboratory and using Solar system tests. If, additionally, there is no direct non-gravitational interaction between DE and DM in the physical reference frame, so that the DE energy-momentum tensor is

covariantly conserved, the density contrast reconstructed in this manner should match that determined directly from observations of large scale structure. In this case the methods developed in this paper will provide an important consistency check on DE models such as Λ and Quintessence. On the other hand, *geometrical* models of DE (Braneworlds, scalar-tensor gravity, etc.) usually predict a different growth rate for $\delta(z)$ from that in general relativity (GR). Models where DE has a direct non-gravitational interaction with DM, or where DE and DM are unified, have a similar property even in the framework of GR. In this case, a reconstruction of the linearized density contrast from observations of standard candles/rulers will not match with δ determined directly from large scale structure (Lue *et al.* 2004; Bertschinger 2006; Ishak *et al.* 2006; Knox *et al.* 2006; Chiba & Takahashi 2007; Huterer & Linder 2007; Wang *et al.* 2007; Mortonson *et al.* 2008; Polarski & Gannouji 2008; Song & Koyama 2008). Currently reconstructed values of the growth rate from galaxy redshift distortions (Guzzo 2008; Verde *et al.* 2002; Hawkins *et al.* 2003; Ross *et al.* 2007) are not very constrictive, but future missions like Euclid (Cimatti *et al.* 2008) are expected to constrain the growth rate tightly. Therefore comparing the results from future supernova data, using the methods described in this paper, to those from future large scale structure data will help address important issues concerning the nature of gravity and dark energy.

This paper is organized as follows. In section 2, we describe the reconstruction technique and the data used to test this method. Section 3 shows the results and examines the dependence of the method on various factors such as the redshift distribution of the data and information on other cosmological parameters. The conclusions are presented in section 4.

2. Methodology

In the longitudinal (quasi-Newtonian) gauge, the perturbed, spatially flat, Friedman-Robertson-Walker (FRW) metric is defined by the line element

$$ds^2 = -(1 + 2\phi)dt^2 + (1 - 2\psi)a^2(t)d\vec{x}^2, \quad (1)$$

where $\phi = \psi$ in GR if matter is free of anisotropic stresses (we assume DM to be cold and neglect small effects from the neutrino component which produces $\phi \neq \psi$). The Newtonian potential ϕ and the non-relativistic matter density contrast

$$\delta_m = \frac{\rho_m(\vec{x}, t) - \bar{\rho}(t)}{\bar{\rho}(t)}, \quad (2)$$

are linked via the linearized Poisson equation

$$k^2\phi = -4\pi G a^2 \rho_m \delta_m. \quad (3)$$

If the DE energy-momentum tensor is covariantly conserved, then $\rho_m \propto a^{-3}$. In this case it is straightforward to show (see, e.g. Wang & Steinhardt 1998; Starobinsky 1998) that on scales much smaller than the effective Jeans scale for DE, $\lambda_J \sim c_s H^{-1}$, where $H(z) \equiv \dot{a}/a$ is the Hubble parameter and c_s is the effective DE sound velocity ($c_s = 1$ for standard quintessence), linearized matter density perturbations in a FRW universe containing DE with an arbitrary effective equation of state $w(t) \equiv p_{DE}/\rho_{DE}$ satisfy the same equation as in the case of a standard FRW model driven by dust and a cosmological constant (Peebles 1980):

$$\ddot{\delta}_m + 2H\dot{\delta}_m - 4\pi G\rho_m\delta_m = 0, \quad (4)$$

(we ignore the subscript in δ_m in the ensuing discussion). However, the generic textbook solution (Peebles 1980; Sahni & Coles 1995)

$$\delta \propto H(z) \int_{z_0}^z \frac{1+z_1}{H^3(z_1)} dz_1 \quad (5)$$

is not applicable now, apart from the following cases: dust-like matter, a non-zero spatial curvature (and/or a tangled network of cosmic strings) and a cosmological constant, for which $H^2(z) = C_1 + C_2(1+z)^2 + C_3(1+z)^3$. The same refers to the other well-known expression valid only for dust and a cosmological constant:

$$\delta \propto a(t) - H(t) \int^t a(t_1) dt_1, \quad (6)$$

see e.g. (Kofman & Starobinsky 1985; Bertschinger 2006).¹ Thus, for an arbitrary physical DE, Eq (4) has to be solved numerically. Since there are no terms depending on the perturbation wave vector \mathbf{k} in it, $\delta(z)/\delta(0)$ will be k -independent, too. We will also suppose that c_s is not too small, so that $k \gg a/\lambda_J$ for all scales of interest, in particular, $c_s \gg 0.01$ if we consider scales up to $100(1+z)^{-1}$ Mpc.

The dimensionless physical distance

$$E = a(t_0)H_0 \int_t^{t_0} \frac{dt}{a(t)} = H_0 \int_0^z \frac{dz_1}{H(z_1)}, \quad (7)$$

where t_0 is the present moment, plays a key role in measurements of the background universe

¹The expression (6) is, in fact, the first term in the long-wave (super-Hubble) expansion of the adiabatic mode of a comoving density perturbation if the perturbed matter pressure tensor is proportional to the unit one and the spatial curvature may be neglected. Then $\phi = \psi = -\zeta(\vec{x}) \left(1 - \frac{H}{a} \int_{t_1}^t a dt\right)$, where the gauge-invariant curvature perturbation ζ does not depend on time for the growing adiabatic mode, see e.g. (Polarski & Starobinsky 1992; Bertschinger 2006). The quantity t_1 is free and may be chosen to coincide with the moment of the first Hubble radius crossing during inflation (another choice would correspond to adding a decaying adiabatic mode with an arbitrary amplitude). Then, using Eq. (3) and the fact that $\rho_m \propto a^{-3}$, the formula (6) follows. Since DE is practically unclustered at sub-Hubble scales, it is tempting to try to use this formula for $\lambda_J \ll \lambda \ll H^{-1}$, too. However, as pointed above, this works only if DE is a cosmological constant.

using standard rulers and candles. E is proportional to the conformal time measured from the present to a moment in the past. It is related to the luminosity distance, d_L , via

$$\frac{H_0 d_L(z)}{1+z} = \frac{1}{\sqrt{|\Omega_K|}} \sin\{\sqrt{|\Omega_K|}E(z)\}, \quad \Omega_K < 0 \quad (8)$$

$$\frac{H_0 d_L(z)}{1+z} = E(z), \quad \Omega_K = 0 \quad (9)$$

$$\frac{H_0 d_L(z)}{1+z} = \frac{1}{\sqrt{\Omega_K}} \sinh\{\sqrt{\Omega_K}E(z)\}, \quad \Omega_K > 0 \quad (10)$$

where $\Omega_K \equiv 1 - \Omega_{\text{total}}$. The following relationship between the luminosity distance d_L and the angular size distance d_A holds in a metric theory of gravity: $d_L = (1+z)^2 d_A$. Rewriting Eq (4) in terms of Eq (7) and using the fact that $\rho_m \propto (1+z)^3$, we obtain:

$$\left(\frac{\delta'}{1+z(E)} \right)' = \frac{3}{2} \Omega_{0m} \delta, \quad (11)$$

where the prime denotes a derivative with respect to E . It is straightforward to transform Eq (11) into the following set of integral equations for $\delta(E)$ and its first derivative (Sahni & Starobinsky 2006):

$$\delta(E) = 1 + \delta'_0 \int_0^E [1+z(E_1)] dE_1 + \frac{3}{2} \Omega_{0m} \int_0^E [1+z(E_1)] \left(\int_0^{E_1} \delta(E_2) dE_2 \right) dE_1 \quad (12)$$

$$\delta'(E) = \delta'_0 [1+z(E)] + \frac{3}{2} \Omega_{0m} [1+z(E)] \int_0^E \delta(E_1) dE_1, \quad (13)$$

where δ is normalized to $\delta_0 \equiv \delta(z=0) = 1$. Note the remarkable fact that, in contrast to formulas used in the reconstruction of $H(z)$ from $d_L(z)$ (Starobinsky 1998; Huterer & Starkman 1999) or $\delta(z)$ (Starobinsky 1998) which require taking a derivative of observational data with respect to the redshift, this formula contains integrations of observational data only, which is a sound operation for noisy data.

By solving the above equations we can calculate the linear *growth factor*

$$g(z) \equiv (1+z)\delta(z), \quad (14)$$

which represents the ratio of $\delta(z)$ in the presence of dark energy to that in SCDM without a cosmological constant. Another quantity of interest is the *growth rate*

$$f(z) = \frac{d \ln \delta}{d \ln a} = -\frac{1+z}{H(z)} \frac{\delta'(E)}{\delta(E)}. \quad (15)$$

To solve Eq (12) we start with initial guess values for $\delta(E)$ and $\delta'(E)$ and iteratively solve for $\delta(E)$, calculating $\delta'(E)$ in the successive iterations as the difference between adjacent values of $\delta(E)$, i.e. $\delta'_i = \Delta\delta_i/\Delta E_i$. For calculating $f(z)$ we require to estimate $H(z)$ as well. We obtain this quantity by differentiating the noisy data $E(z)$ using a finite differencing method. This naturally amplifies the noise in the final results, so we expect the results for $f(z)$ to be slightly noisier. However, typically the difference in $f(z)$ between two models of dark energy is greater than the difference in $g(z)$, so despite the greater noise, we expect $f(z)$ to be useful for discriminating dark energy models. This method does not require prior knowledge of the parameter δ'_0 , is robust to changes in the initial guess values and gives exact results for $g(E)$ and $f(E)$ for noiseless data. For data with errors, naturally the result is noisier, however, as we will show in the succeeding sections, we will be able to put reasonable constraints on g and f using this method.

Data noise can also be decreased using smoothing techniques. In what follows we shall use the lognormal smoothing scheme proposed in (Shafieloo *et al.* 2006) which has been shown to be reasonably unbiased and efficient. It constructs a smooth quantity, E^s , from a noisy one, $E(z_i)$, via the ansatz (Shafieloo *et al.* 2006)

$$E^s(z) = \sum_i E(z_i) \exp\left(\frac{-\ln^2 \frac{1+z_i}{1+z}}{2\Delta^2}\right) / \sum_i \exp\left(\frac{-\ln^2 \frac{1+z_i}{1+z}}{2\Delta^2}\right), \quad (16)$$

where Δ is the smoothing scale (see also Shafieloo 2007). We take $\Delta \simeq 1/N$ where N is the total number of observations. Choosing this small value of Δ leaves the results unbiased.

From the manner in which Eqs (11-13) have been obtained, reasons as to why the linearized growth function $\delta_{\text{obs}}(z)$ determined from actual observations of large scale structure may differ from $\delta(z)$ reconstructed using our method follow immediately:

1. ρ_m is not proportional to $(1+z)^3$. This happens even in GR if the energy-momentum tensor of physical DE is not covariantly conserved separately, either due to the existence of a direct non-gravitational interaction between DE and DM (see Amendola 1999; Billyard & Coley 2000; Zimdahl & Pavon 2001; Caldera-Cabral *et al.* 2008, and references therein), or because DE and DM constitute some unique entity as occurs in unified DM–DE models such as the Chaplygin gas (Kamenshchik *et al.* 2001) and its generalizations. In such models DE is partially clustered with DM on small scales, and this can result in the appearance of significant k -dependent terms in the equation for δ , so that the growth factor $g(z)$ becomes k -dependent. In particular, the latter effect is especially crucial for the generalized Chaplygin gas model, (see the recent paper Gorini *et al.* 2008, and references to previous papers therein).

2. GR is modified, DE is geometrical. Then G in Eq (4) becomes some effective quantity G_{eff} which may be both time and scale dependent. A noticeable value of $\phi - \psi$ may also arise even in the absence of free-streaming particles. However on small scales this value is strongly restricted by Solar system tests of gravity (which don't suggest any such effect). Geometrical models of DE, which include Braneworld models and models using scalar-tensor and $f(R)$ gravity, have more degrees of freedom than GR, so it is natural that in this case, the linearized perturbation equation for δ shows a departure from the Newtonian form, Eq (4). For instance in extra dimensional scenario's (Dvali *et al.* 2000; Sahni & Shtanov 2003), the presence of the fifth dimension (the bulk) can influence the behaviour of perturbations residing on the brane (Lue *et al.* 2004; Koyama & Maartens 2006; Sawicki *et al.* 2007; Shtanov *et al.* 2007) making them significantly k -dependent even on scales much smaller than the Hubble distance (Shtanov *et al.* 2007). The same effect arises in viable DE models in $f(R)$ gravity (Hu & Sawicki 2007; Starobinsky 2007; Tsujikawa *et al.* 2008) (see the recent review Sotirou & Faraoni 2008, for numerous papers on $f(R)$ gravity as a whole).

On the other hand, in some cases G_{eff} and $g(z)$ may remain scale-independent even on small scales, though they acquire a non-trivial, non-GR, time dependence. This occurs, for instance, in the Dvali-Gabadadze-Porrati (DGP) extra-dimensional model considered below as well as in scalar-tensor DE models with a large current value of the Brans-Dicke parameter ω_{BD} (Boisseau *et al.* 2000; Gannouji & Polarski 2008).

Thus, a comparison of the observed and reconstructed density contrast could help shed light on the nature of dark energy. While it is encouraging that future observations (Blake 2004; Guzzo 2008; Song 2008; Cimatti *et al.* 2008) of large scale structure may make possible the determination of $\delta_{obs}(z)$, in this paper we focus on reconstructing δ using observations of high redshift type Ia supernovae and baryon acoustic oscillations.

2.1. Data used

The method outlined in the previous section would be applicable to any observation which contains a measurement of $E(z)$, e.g. measurements of luminosity distance or angular diameter distance. We shall use real data and mock data based on simulations of supernova type Ia data and the angular diameter distance from baryon acoustic oscillations, to test this method.

Supernova Data :

The lightcurves of Type Ia supernovae show them to be “calibrated candles”, therefore they are of enormous significance in cosmology today. The luminosity distance of Type Ia SNe provide us with a direct measurement of the acceleration of the universe, thus leading to constraints on the dark energy parameters. SNe data is in the form $\{m_B, z, \sigma_{m_B}, \sigma_z\}$, where the magnitude m_B is related to $d_L(z)$ as

$$m_B = 5\log_{10}[H_0 d_L(z)] + \mathcal{M} , \quad (17)$$

\mathcal{M} being a noise parameter usually marginalized over.

It should be noted that supernova data, on its own, is unable to break the degeneracy between dark energy and spatial curvature. The CMB, on the other hand, places stringent constraints on Ω_K and strongly suggests that the universe is spatially flat, in agreement with predictions made by the inflationary scenario. In this paper we shall work under the assumption that $\Omega_K = 0$ and use (9) to relate $d_L \rightarrow E(z)$, with the latter playing the key role in our reconstruction exercise (12).

Currently there are around 300 published SNe with the furthest observed one at a redshift of $z = 1.7$ (Kowalski 2008), and average error of $\sigma_{m_B} \simeq 0.15$. Future space-based projects such as the Joint Dark Energy Mission (JDEM) (JDEM collaboration) are expected to observe about 2000 SNe with errors of $\sigma_{m_B} = 0.07$. To date, SNe are the most direct evidence for dark energy, and in this paper we shall primarily use SNe data to constrain the growth parameters for different dark energy models.

BAO data

At present, baryon acoustic oscillations are believed to be the method least plagued by systematic uncertainties, therefore the detection of the first baryon acoustic oscillation scale (Eisenstein *et al.* 2005) has led to the speculation that BAO may in future become a potent discriminator for dark energy. Standing sound waves that propagate in the opaque early universe imprint a characteristic scale in the clustering of matter, providing a “standard ruler”. Since the sound horizon is tightly constrained by cosmic microwave background (CMB) observations, measuring the angle subtended by this scale determines a distance to that redshift and constrains the expansion rate. The radial and transverse scales give measurements of $[r_s H(z)]/c$ and $r_s/[(1+z)d_A(z)]$ respectively, where r_s is the sound horizon obtained from CMB. These quantities are correlated, and the present BAO data is not sensitive enough to measure both quantities independently (see however the recent papers Benitez *et al.* 2008; Gaztanaga *et al.* 2008), but future surveys are expected to give independent measurements of $d_A(z)$ and $H(z)$ (Seo & Eisenstein 2003). Future

BAO surveys such as BOSS (SDSS collaboration) should therefore place tighter constraints on dark energy parameters.

3. Results

We first use Supernova data to reconstruct the growth parameters. We simulate data according to two theoretical models :

- Model 1 : A cosmological constant model with $w = -1, \Omega_{0m} = 0.27, H_0 = 72$ km/s/Mpc.
- Model 2: A variable dark energy model with the equation of state given by

$$w(z) = w_0 + \frac{w_a z}{1+z}, \quad w_0 = -0.9, \quad w_a = 0.3, \quad (18)$$

and with the same values of Ω_{0m}, H_0 as Model 1. Note that the Models 1 and 2 provide excellent agreement with the current CMB+BAO+SNe data (Komatsu *et al.* 2008).

The Model 2 has $w > -1$ everywhere, so it can be realized by quintessence with some potential for which Eq (4) is valid.

Two different data distributions are used, set A resembles the quality of data available at present, and set B is modeled on expected future surveys.

- Set A : ~ 300 SNe, with the redshift distribution and errors of the Union dataset (Kowalski 2008). For this dataset, on average, $\sigma_{m_B} \simeq 0.15$, but a few SNe have very high errors of the order of unity. Since the method of integration would not work very well for very noisy data, and a single datapoint with large noise would affect the results of all datapoints after it, we restrict the analysis to SNe with $\sigma_{m_B} < 0.7$. By rejecting only 10 datapoints with this criterion, we enhance the results by a significant amount.

- Set B : ~ 2000 SNe, with the redshift distribution and errors ($\sigma_{m_B} \sim 0.07$) expected from future surveys such as the JDEM (Aldering *et al.* 2004). The data covers a redshift range of $z = 0.1 - 1.7$ with a larger concentration of supernovae in the midrange redshifts ($z = 0.4 - 1.1$). The errors considered here are statistical only, we do not consider systematic errors, which are expected to be better controlled in the future with larger datasets.

For both cases, we marginalize over $\Omega_{\text{dm}} = 0.27 \pm 0.03$. Supernova data is unable to break the degeneracy between dark energy and curvature of the universe. In order to measure the growth parameters, we therefore consider only a flat universe, which is the preferred model from current CMB observations.

Fig 1 shows the results for the linear growth factor $g(z)$ for both datasets and for the two different cosmological models. We see that for both models, set A results in rather noisy reconstruction (left panel), since the errors on the SNe are quite high. This is especially true at high redshifts ($z > 0.7$) where the sparse sampling affects the integral reconstruction scheme adversely. At $z = 0.3$, $g(z)$ is constrained to $\sim 5\%$. For JDEM-like data (set B) however, $g(z)$ is reconstructed more accurately, and has low errors at low redshifts (right panel). At $z = 0.3$, $g(z)$ is constrained accurately to $\sim 2\%$ for both models for set B, while at $z = 1$, $g(z)$ is constrained to $\sim 4\%$.

Fig 2 shows the reconstruction of the growth rate $f(z)$. As before, the results for set A are poor, with $f(z)$ constrained to $\sim 6\%$ at $z = 0.3$. The results for Set B are reasonable, however, the errors are slightly larger in this case than for $g(z)$, since there is an additional error from the calculation of $H(z)$ from $E(z)$. At $z = 0.3$, $f(z)$ is constrained accurately to $\sim 3\%$ for both models for set B, while at $z = 1$, $f(z)$ is constrained to $\sim 8\%$. We also note that the quantity $f(z)$ has slightly greater discriminatory power than $g(z)$, since typically the growth factor shows rather less variation between different dark energy models as compared to the growth rate at any given redshift. Therefore, even though $f(z)$ is slightly

noisier, for set B, Model 1 and Model 2 can be discriminated at 1σ using $f(z)$.

If the data is first smoothed with the smoothing scheme, Eq (16), the results improve, especially for set A which has much noisier data, as seen in figure 3. The results for $f(z)$ improve markedly for both datasets. This is because an additional quantity $H(z)$ is required for obtaining $f(z)$, and a smoother $E(z)$ leads to a much more accurate estimation of $H(z)$. Errors on $g(z)$ and $f(z)$ are $\sim 1\%$ and $\sim 1.5\%$ respectively at $z = 0.3$, and $\sim 3\%$ and $\sim 6\%$ respectively at $z = 1$ for Model 1 with JDEM like data. Model 2 gives similar constraints. The results for the growth parameters are summarized in Table 1 for Model 1, and in Table 2 for Model 2. We see that this method obtains quite reasonable constraints on the growth parameters at low redshifts for the set B, therefore it can be used successfully to constrain growth parameters from future SNe data. It should be noted that, for future SNe data to accurately constrain the growth parameters, it is important to keep the SNe systematics under control ($\sigma_{sys} \lesssim 0.05$). A systematic error of $\sigma_{sys} = 0.1$ (as on the current data) would weaken all constraints significantly.

3.1. Dependence on nature of data

We now check how the results change if the redshift distribution or error distribution is changed. To study the dependency on the number of SNe, we use three redshift distributions– (a) set A (~ 300 SNe) with double the number of supernovae at low ($z < 0.3$) and high ($z > 0.7$) redshifts, (b) set A with double the SNe at mid-range ($0.3 < z < 0.7$) redshifts, and (c) a distribution with the JDEM (set B) redshift distribution (~ 2000 SNe) with errors of the order of the Union (set A) SNe. The results for Model 1 are shown in figure 4. We see that doubling the number of SNe in a particular redshift bin changes the results very slightly. This is to be expected because when integrating noisy data, having a larger number of points with the same amount of noise does not improve results significantly. Increasing the total number of SNe by a significant amount (nearly seven

times, as in right panel) does improve the scatter, but the results still do not compare with those of set B (fig 2, top right panel) which has the same number of supernovae but smaller errors.

We now study the effect of the errors. Once again we study three distributions — (a) set A with the errors halved for $z < 0.3$ and $z > 0.7$ redshift bins, (b) set A with errors halved in the $0.3 < z < 0.7$ redshift bin, and (c) set A with errors replaced by JDEM-like errors on all SNe. The results for Model 1 are shown in figure 5. We see that in this case, decreasing the errors at low redshift or high redshift changes the results very slightly. This is because there are very few points at low redshift so they do not affect the integration process strongly, while the high redshift points cannot affect the low redshift points. The results in the redshift range $0.3 < z < 0.7$ become better if the mid-range SNe have lower errors. As we see in the right panel of fig 5, decreasing the errors to JDEM errors gives results almost identical to the results for Set B (fig 2, top right panel) , even though the number of points is much less for set A. Thus we find that this method would work quite well even for a reasonable number of supernovae (of the order of a few hundred) provided the errors were tightly constrained.

Since the high errors of set A make it unsuitable for this reconstruction approach, in the next sections we will use the set B to study the robustness of the results to various other factors.

3.2. Growth rate from $w(z)$

We may also calculate the growth rate f from the supernova data via the equation of state using the following approximation (Wang & Steinhardt 1998) :

$$f(z) \simeq \Omega_m(z)^\gamma = \left[\frac{\Omega_{0m}(1+z)^3}{H^2(z)} \right]^\gamma \quad (19)$$

$$\gamma(z) = \frac{3}{5 - \frac{w}{1-w}} + \frac{3}{125} \frac{(1-w)(1 - \frac{3}{2}w)}{(1 - \frac{6}{5}w)^3} (1 - \Omega_m(z)) + \mathcal{O}[(1 - \Omega_m(z))]^2, \quad (20)$$

where the equation of state $w(z)$ may be calculated using a likelihood parameter estimation from the luminosity distance. This approximation works quite well for a large number of physical dark energy models with a constant or slowly changing w including LCDM, for which $\gamma \simeq 0.55$ (Wang & Steinhardt 1998; Linder 2005). We use the familiar CPL fit (Chevallier & Polarski 2001; Linder 2003) :

$$w(z) = w_0 + \frac{w_a z}{1+z}, \quad (21)$$

$$H^2(z) = H_0^2 [\Omega_{0m}(1+z)^3 + (1 - \Omega_{0m})(1+z)^{3(1+w_0+w_a)} e^{3w_a(1/(1+z)-1)}] . \quad (22)$$

A likelihood parameter estimation is expected to lead to smaller errors, but the drawback of this method is that the result may be biased due to the parameterization. Also the errors on $w(z)$ would propagate extremely non-linearly to f and therefore the result for $f(z)$ would be much less trustworthy.

Figure 6 shows the reconstructed $f(z)$ for Model 1 and 2 for set B. As expected, the errors are lower than those for our reconstruction method. However, it is also noteworthy that the resulting confidence levels are *not symmetric* around the true value, in fact at higher redshifts, the true model appears to be on the verge of being ruled out ! These results are commensurate with those found in (Mortonson *et al.* 2008), where reconstruction of the growth parameters through w leads to biases in the growth parameter results even though w is recovered accurately. This is due to the fact that errors propagate non-linearly from w to $f(z)$. We therefore conclude that, when reconstructing the growth parameters from supernova data, it is better to reconstruct the quantities directly, rather than reconstructing them indirectly from the energy density or equation of state.

3.3. Dependence on Ω_{0m}

Supernova data do not simultaneously constrain information on Ω_{0m} and dark energy parameters. To reconstruct dark energy parameters, it is necessary to place constraints on

Ω_{0m} from other observations. In the calculations so far, we have marginalized over the true fiducial value for Ω_{0m} . However, since there is considerable uncertainty as to the real value of the matter density, we check how using *incorrect* values of Ω_{0m} may bias our analysis. (It is well known that an incorrect value of Ω_{0m} can significantly bias the results for DE (Shafieloo *et al.* 2006; Sahni *et al.* 2008).) The fiducial universe for model 1 contains $\Omega_{0m} = 0.27$. We now choose a different, incorrect, value of $\Omega_{0m} = 0.3$ for marginalization and proceed to analyze the data using both the integral reconstruction method and the likelihood parameter estimation of w outlined in the previous section. The results are shown in figure 7. We see that choosing a higher value of Ω_{0m} gives biased results in both methods, but interestingly enough, the biases are in *opposite directions* ! In case of the integral reconstruction method, a higher value of Ω_{0m} leads to a lower value of $f(z)$ at high redshifts, whereas for the w parameterization, a higher value of Ω_{0m} leads to a higher value of $f(z)$.

These results may be understood as follows. For the reconstruction from w , we see from eq (19) that $f(z)$ changes primarily due to the change in the matter density $\Omega_{0m}(1+z)^3$, since the value of γ does not vary very strongly with w , and $H^2(z)$ is constrained by the data. Choosing a higher value of Ω_{0m} would result in the choice of a different $w(z)$ which would lead to nearly the same $H(z)$ as that for a lower value of Ω_{0m} , and γ would also not change by much. However, the quantity $\Omega_{0m}(1+z)^3$ would increase proportionate to Ω_{0m} . Therefore a higher value of Ω_{0m} would simply result in a higher value of $f(z)$. In the case of the integral reconstruction however, we see from eq (12) that both δ and δ' depend on Ω_{0m} . In δ the leading term is unity and the other two terms containing δ'_0 and Ω_{0m} are at about an order of magnitude smaller. In δ' the two terms containing δ'_0 and Ω_{0m} are of the same order and opposite sign. The Ω_{0m} term contributes by making δ' less negative. Therefore increasing Ω_{0m} increases δ slightly and decreases the absolute value of δ' by a larger amount, so that the ratio between δ and δ' becomes a smaller negative quantity.

Since $f(z)$ is essentially this ratio, this means that $f(z)$ also decreases with increasing Ω_{0m} . Therefore, choosing a wrong value of Ω_{0m} causes the two different methods of reconstruction to be biased in opposite directions. This leads to the interesting conclusion that, provided other systematics are under control, comparing the integral reconstruction method with the standard likelihood estimation would give us a valuable consistency check on the accuracy of the prior chosen for Ω_{0m} .

3.4. Reconstruction for a toy modified gravity model

An influential Braneworld model was suggested by Dvali-Gabadadze-Porrati (Dvali *et al.* 2000). The expansion history for this model is given by

$$H(z) = H_0 \left[\left(\frac{1 - \Omega_{0m}}{2} \right) + \sqrt{\Omega_{0m}(1+z)^3 + \left(\frac{1 - \Omega_{0m}}{2} \right)^2} \right]. \quad (23)$$

For physical models of dark energy, the growth rate is well approximated by eq (19), for instance $\gamma \simeq 0.55$ for LCDM (Wang & Steinhardt 1998; Linder 2005; Peacock *et al.* 2001; Thomas *et al.* 2008; Acquaviva *et al.* 2008). This equation is not valid however if the observed acceleration originates from a modification of the equations of general theory of relativity; in the DGP Braneworld theory, the growth rate is approximated by (Lue *et al.* 2004)

$$f(z) \simeq \Omega_m(z)^{0.68}. \quad (24)$$

This is the growth rate which would be measured through galaxy redshift distortions or weak gravitational lensing, whereas any analysis from the expansion history would obtain a growth rate commensurate with eq (19).

Therefore, if the growth rate for this model is reconstructed using on the one hand, supernova data, and on the other, galaxy redshift distortions, we expect the results to be different. We reconstruct the growth rate using the JDEM-like SNe distribution for this

modified gravity model by substituting Eq (23) into the integral reconstruction method described by Eq (12). The result is shown in figure 8. For comparison, we have also plotted the expected observational constraints from galaxy redshift distortions for the future Euclid mission (Cimatti *et al.* 2008). We see that the two results are strongly discrepant, especially at low redshifts. If the origin of dark energy were indeed geometrical in nature, comparisons of this sort would provide crucial evidence for it.

Despite the popularity of the DGP model, it is currently facing several difficulties both of an observational and theoretical nature: Tension between this model and observational data sets has been pointed out in (Fairbairn & Goobar 2006; Alam & Sahni 2006; Alam & Sahni 2002; Maartens & Majoretto 2006) and the presence of a ghost in DGP gravity (Charmousis *et al.* 2006; Gregory *et al.* 2007; Deffayet *et al.* 2006; Koyama 2007) may be even more problematic. Consequently our purpose in the present section has been to treat DGP cosmology as a toy model, used to demonstrate the utility of the reconstruction approach developed in this paper. (Note however the existence of other braneworld models which are ghost free (Sahni & Shtanov 2003; Shtanov *et al.* 2009) and agree well with observations (Alam & Sahni 2006).)

3.5. Current SNe Data

In figure 9 we show the reconstructed growth parameters for the currently available supernova data– the Union dataset (Kowalski 2008). The results are marginalized over $\Omega_{0m} = 0.26 \pm 0.03$, the currently accepted value of Ω_{0m} (Dunkley *et al.* 2008). The nuisance parameter \mathcal{M} which contains information on H_0 is also marginalized over. For the non-smoothed method, since errors are quite large, it is difficult to put any constraints on the growth parameters. If the smoothing scheme is used, $f(z)$ may be constrained to $\sim 6\%$ at $z = 0.3$. At this redshift, the growth factor $g(z)$ would be constrained to $\sim 5\%$. The reconstructed $f(z)$ is commensurate with the cosmological constant model as well as Model 2

(variable w , eq (18)) used in this paper. We also show the three current observations of $f(z)$ from galaxy redshift-space distortions (Guzzo 2008; Verde *et al.* 2002; Ross *et al.* 2007). The error bars on these observations are at present quite large, but it is expected that future data in this field would be comparable with our results from supernovae, thus we would be able to discern physical and geometrical DE using these different techniques (as shown in section 3.4). Table 3 shows the 1σ limits on the growth parameters for the reconstruction.

3.6. Data expected from future BAO experiments

We now check the method with BAO data. The SDSS baryon acoustic oscillation survey of BOSS is expected to measure the baryon acoustic oscillation power spectrum very accurately. The expected accuracy on the angular diameter distance d_A is of the order of 1.0% at $z = 0.35$, 1.1% at $z = 0.6$, and 1.5% at $z = 2.5$, with errors on $H(z)$ of 1.8%, 1.7% and 1.5% at the same redshifts (SDSS collaboration). We populate a redshift range of $z = 0.2 - 2.5$ with 20 datapoints with errors based on these numbers and use this dataset to reconstruct the growth parameters. Since there are only 20 points in the dataset, and not many at very low redshifts, the integration is not very accurate even though the errors on d_A and H are small. We find that for this dataset $g(z)$ and $f(z)$ are both constrained to $\sim 9\%$ at $z = 2.5$ (see Tables 1 and 2, bottom row). Although these errors appear to be large compared to those from the SNe data, for a high redshift of $z = 2.5$, these errors are actually commensurate to the errors from SNe. The advantage of using the BAO is that we obtain the growth parameters at a higher redshift, which is complementary to the SNe results. In the future, if systematics are controlled, and probes like JDEM are able to measure both SNe and BAO data, we should be able to obtain independent estimates of the growth parameters at both very low and very high redshifts from this method.

4. Conclusions

In this paper we have proposed a method for extracting growth parameters for dark energy models (within the spatially flat FRW universe) from observations that map the background universe, such as measures of the luminosity distance or the angular diameter distance. The method is model independent and unbiased. For current data, the growth factor $g(z)$ may be constrained to $\sim 5\%$ at $z = 0.3$, while the growth rate $f(z)$ is constrained to $\sim 6\%$. For future JDEM SNe data, we will be able to put constraints of the order of a few percent on the growth parameters, e.g. 2% on the growth factor and 3% on the growth rate at a redshift of 0.3 , and 4% on the growth factor and 8% on the growth rate at a redshift of unity. In conjunction with the likelihood parameter estimation method, this method acts as an important consistency check on the accuracy of the priors on Ω_{0m} for SNe. With future probes like JDEM and BOSS taken in conjunction, it will lead to an unbiased estimation of the growth parameters upto a redshift of $z = 2.5$.

It is well known that, in GR and for most DE models, the expansion history completely determines the linearized growth rate of density perturbations (Starobinsky 1998; Sahni & Starobinsky 2006) (the exact conditions for this are formulated at the beginning of Sec. II). Consequently, a comparison of the density contrast reconstructed from the expansion history would provide one more important consistency check for a large variety of DE models including the cosmological constant and quintessence. On the other hand, as explained in more detail at the beginning of Sec. II, any departure of the observed density contrast from that reconstructed using standard candles and rulers would almost certainly indicate that either there is an exchange of energy between DE and DM (so that the effective energy-momentum tensor of DE is not on its own covariantly conserved), or that cosmic acceleration is a consequence of modified, non-Einsteinian gravity. In modified gravity theories, such as Braneworld models, scalar-tensor and $f(R)$ gravity, etc., the linearized perturbation equation for δ does not follow the Newtonian form, Eq (4) (Lue *et al.* 2004;

Koyama & Maartens 2006; Shtanov *et al.* 2007; Hu & Sawicki 2007; Boisseau *et al.* 2000; Jain & Zhang 2007; Song & Koyama 2008; Zhao *et al.* 2008; Song & Dorè 2008). Hence the density contrast reconstructed using observations of standard candles/rulers via Eq (12) and the density contrast determined directly from observations of large scale structure, say, by weak lensing, galaxy redshift distortions or cluster abundances at different z (Guzzo 2008; Song 2008; Vikhlinin 2008; Cimatti *et al.* 2008), are likely to differ.

In Sec. 3.4 we show that one can obtain a strong signature of modified gravity by comparing results of this reconstruction method with future observations of galaxy redshift distortions using the DGP model as a toy example of modified gravity, where the growth factor $g(z)$ is scale-independent on small scales. However, as discussed in Sec. II, $g(z)$ often becomes scale-dependent both in modified gravity and in the case of direct DE–DM interaction (or their unification). Therefore, for further discrimination of DE models alternative to quintessence and the cosmological constant, measurement of δ at different comoving scales is required to determine if $g(z)$ is scale-dependent or not.

Future surveys such as JDEM are expected to deliver high quality data for both supernovae and weak lensing. Using such surveys it would then be possible to compare the reconstructed density contrast from standard candles (SNe) with the density contrast observed from gravitational clustering (lensing). Therefore, we hope that the techniques developed in this paper, combined with future observations, will help unravel the nature of that most enigmatic quantity – dark energy.

5. Acknowledgements

AAS acknowledges RESCEU hospitality as a visiting professor. He was also partially supported by the grant RFBR 08-02-00923 and by the Scientific Programme “Astronomy” of the Russian Academy of Sciences. UA acknowledges support from the LDRD program at Los Alamos National Laboratory and useful discussions with S. Habib, D. Holz and Z.

Lukic.

REFERENCES

- Acquaviva, V., Hajian, A., Spergel, D. N., & Das, S. 2008, Phys. Rev. D **78**, 043514
- Alam, U. & Sahni, V. 2002, astro-ph/0209443
- Alam, U., Sahni, V., & Starobinsky, A. A. 2004, J. Cosmol. Astropart. Phys. **0406** 008
- Alam, U. & Sahni, V. 2006, Phys. Rev. D **73**, 084024
- Alam, U., Sahni, V., & Starobinsky, A. A. 2007, J. Cosmol. Astropart. Phys. **0702** 011
- Aldering, G., *et al.* , 2004, arXiv:astro-ph/0405232
- Amendola, L. 1999, Phys. Rev. D **60**, 043501
- Astier, P., *et al.* , 2005, Astron. Astroph. **447**, 31
- Benitez, N., *et al.* , 2008, arXiv:0807.0535
- Bertschinger, E. 2006, Astroph. J. **648**, 797
- Billyard, P., & Coley, A. 2000, Phys. Rev. D **61**, 083503
- Blake, C. A., Abdallah, F. B., Bridle, S. L. & Rawlings, S. 2004, In "Science with the Square Kilometer Array", eds. C. Carilli and S. Rawlings, New Astronomy Reviews (Elsevier: Amsterdam), 2004, arXiv:astro-ph/0409278
- Boisseau, B., Esposito-Farese, G., Polarski, D., & Starobinsky, A. A. 2000, Phys. Rev. Lett. **85**, 2236
- Caldera-Cabral, G., Maartens, R., & Urena-Lopez, L. A. 2008, arXiv:0812.1827
- Carroll, S. M. 2001, Living Rev.Rel. **4**, 1
- Charmousis, C., Gregory, R., Kaloper, N., & Padilla, A. 2006, JHEP **0610**, 066

Chevallier, M., & Polarski, D. 2001, *Int. J. Mod. Phys. D* **10**, 213

Chiba, T. & Takahashi, R. 2007, *Phys. Rev. D* **75**, 101301.

Cimatti, A., *et al.* , 2008, [arXiv:0804.4433](https://arxiv.org/abs/0804.4433);

<http://sci.esa.int/science-e/www/object/index.cfm?fobjectid=42266>;

http://hetdex.org/other_projects/euclid.php

Copeland, E. J., Sami, M., & Tsujikawa, S. 2006, *Int. J. Mod. Phys. D* **15**, 1753

Corasaniti, P. S., Bassett, B. A., Ungarelli, C., & Copeland, E. J. 2003, *Phys. Rev. Lett.* **90**,
091303

Deffayet, C., Gabadadze, G., & Iglesias, A. 2006 *J. Cosmol. Astropart. Phys.* **0608**, 012

Dunkley, J. *et al.* 2008, [arXiv:0803.0586](https://arxiv.org/abs/0803.0586).

Dvali, G., Gabadadze, G., & Porrati, M. 2000, *Phys. Lett. B* **485**, 208.

Eisenstein, D. J., *et al.* , 2005, *Astroph. J.* **633**, 560.

Fairbairn, M. & Goobar, A. 2006, *Phys. Lett. B* **642**, 432

Gannouji, R., & Polarski, D. 2008, *J. Cosmol. Astropart. Phys.* **0805**, 018

Gaztanaga, E., Miquel, R., & Sanchez, E. 2008, [arXiv:0808.1921](https://arxiv.org/abs/0808.1921)

Gorini, V., *et al.* , 2008, *J. Cosmol. Astropart. Phys.* **0802**, 018

Gregory, R., Kaloper, N., Myers, R. C., & Padilla, A. 2007, *JHEP* **0710**, 069

Guzzo, L., *et al.* , 2008, *Nature* **451**, 541

Hawkins, E., *et al.* , 2003, *Mon. Not. Roy. Ast. Soc.* **346**, 78

Hu, W. & Sawicki, I. 2007, *Phys. Rev. D* **76**, 064004

- Huterer, D., & Linder, E. 2007, Phys. Rev. D **75**, 023519
- Huterer, D., & Turner, M. S. 1999, Phys. Rev. D **60**, 081301
- Huterer, D., & Starkman, G. 2003, Phys. Rev. Lett. **90**, 031301
- Ishak, M., Upadhye, A., & Spergel, D. 2006, Phys. Rev. D **74**, 043513
- Jain, B & Zhang, P. 2007, arXiv:0709.2375
- Jassal, H. K., Bagla, J. S., & Padmanabhan, T. 2005, Mon. Not. Roy. Ast. Soc. **356**, L11
- JDEM collaboration : <http://universe.nasa.gov/program/probes/jdem.html>
- Kamenshchik, A. Yu., Moschella, U, & Pasquier, V. 2001, Phys. Lett. B **511**, 265
- Knox, L., Song, Y-S. & Tyson, A.J 2006, Phys. Rev. D **74**, 023512
- Kofman, L. A., & Starobinsky, A. A. 1985, Sov. Astron. Lett. **11**, 271
- Komatsu, E., *et al.* , 2008, arXiv:0803.0547
- Kowalski, M., *et al.* , 2008, arXiv:0804.4142
- Koyama, K. 2007, Class. Quantum Grav. **24**, R231
- Koyama, K., & Maartens, R. 2006, J. Cosmol. Astropart. Phys. **0601**, 016
- Lazkoz, R., Nesseris, S., & Perivolaroupolos, L. 2006, Phys. Rev. D **74**, 103505
- Linder, E. V. 2003, Phys. Rev. Lett. **90**, 091301
- Linder, E. V. 2005, Phys. Rev. D **72**, 043529
- Lue, R., Scoccimarro, R., & Starkman, G. D. 2004, Phys. Rev. D **69**, 124015
- Maartens, R., & E. Majerotto, E. 2006, Phys. Rev. D **74**, 023004

- Mortonson, M. J., Hu, W., & Huterer, D. 2008, [arXiv:0810.1744](#)
- Nojiri, S., & Odintsov, S. D. 2007, *Int. J. Geom. Meth. Mod. Phys.* **4**, 115
- Padmanabhan, T. 2003, *Phys. Rep.* **380**, 235
- Peacock, J. A. *et al.* , 2001, *Nature* **410**, 169
- Peebles, P. J. E. 1980, *The Large scale structure of the universe*, Princeton University press
- Peebles, P. J. E., & Ratra, B. 2003, *Rev.Mod.Phys.* **75**, 559
- Percival, W. J., & White, M. 2008, [arXiv:0808.0003](#)
- Perlmutter, S. J., *et al.* , 1998, *Nature* **391**, 51
- Perlmutter, S. J., *et al.* , 1999, *Astroph. J.* **517**, 565
- Polarski, D., & Gannouji, R. 2008, *Phys. Lett. B* **660**, 439
- Polarski, D., & Starobinsky, A. A. 1992, *Nucl. Phys.* **385**, 623
- Rapetti, D., Allen, S. W., Mantz, A., & Ebeling, H. 2008, [arXiv:0812.2259](#)
- Riess, A. G., *et al.* , 1998, *Astron. J.* **116**, 1009
- Riess, A. G., *et al.* , 2005, *Astroph. J.* **607**, 665
- Riess, A. G., *et al.* , 2007, *Astroph. J.* **659**, 98
- Ross, N. P., *et al.* , 2007, *Mon. Not. Roy. Ast. Soc.* **381**, 573
- Sahni, V. & Coles, P. 1995, *Phys. Rept.* **262**, 1
- Sahni, V. & Shtanov, Yu. 2003, *J. Cosmol. Astropart. Phys.* **0311**, 014
- Sahni, V., & Starobinsky, A. A. 2000, *Int. J. Mod. Phys. D* **9**, 373

- Sahni, V., & Starobinsky, A. A. 2006, *Int. J. Mod. Phys. D* **15**, 2105
- Sahni, V., Shafieloo, A., & Starobinsky, A. A. 2008, *Phys. Rev. D* **78**, 103502
- Saini, T. D., Weller, J., & Bridle, S. L. 2004, *Mon. Not. Roy. Ast. Soc.* **348**, 603
- Sarkar, D., *et al.* , 2008, *Phys. Rev. Lett.* **100**, 241302
- Sawicki, I., Song, Y. S., & Hu, W. 2007, *Phys. Rev. D* **75**, 064002
- SDSS collaboration : <http://www.sdss3.org/>; <http://cosmology.lbl.gov/BOSS/>;
http://www-physics.lbl.gov/physdiv/div-office/2006_dir_review/Schlegel.pdf
- Seo, H. S., & Eisenstein, D., J. 2003, *Astroph. J.* **598**, 720
- Shafieloo, A., Alam, A., Sahni, V., & Starobinsky, A. A. 2006, *Mon. Not. Roy. Ast. Soc.* **366**,
1081
- Shafieloo, A. 2007, *Mon. Not. Roy. Ast. Soc.* , **380**, 1573
- Shtanov, Yu., Viznyuk, A., & Sahni, V. 2007, *Class. Quantum Grav.* **24**, 6159
- Shtanov, Yu., Sahni, V., Shafieloo, A. & Toporensky, A. 2009, *J. Cosmol. Astropart. Phys.* **0904**, 023
- Song, Y. S., & Percival, W. J. 2008, [arXiv:0807.0810](https://arxiv.org/abs/0807.0810)
- Song, Y. S., & Dorè, O. 2008, [arXiv:0812.0002](https://arxiv.org/abs/0812.0002)
- Song, Y. S., & Koyama, K. 2008, [arXiv:0802.3897](https://arxiv.org/abs/0802.3897)
- Sotiriou, T., P., & Faraoni, V. 2008, [arXiv:0805.1726](https://arxiv.org/abs/0805.1726)
- Starobinsky, A. A. 1998, *JETP Lett.* **68**, 757
- Starobinsky, A. A. 2007, *JETP Lett.* **86**, 157

Thomas, S. A., Abdalla, F. B., & Weller, J. 2008, [arXiv:0810.4863](#)

Tonry, J. L., *et al.* , 2003, *Astroph. J.* **594**, 1

Tsujikawa, S., *et al.* , 2008, *Phys. Rev. D* **77**, 103009.

Verde, L., *et al.* , 2002, *Mon. Not. Roy. Ast. Soc.* **335**, 432

Vikhlinin, A., *et al.* , 2008, [arXiv:0812.2720](#)

Wang, Y., & Mukherjee, P. 2006, *Astroph. J.* **650**, 1

Wang, L., & Steinhardt, P. J. 1998, *Astroph. J.* **508**, 483

Wang, S., Hui, L., May, M., & Haiman, Z. 2007, *Phys. Rev. D* **76**, 063503

Wood-Vasey, W. M., *et al.* , 2007, *Astroph. J.* **666**, 694

Zhao, G. B., Pogosian, L., Silvestri, A., & Zylberberg, J. 2008, [arXiv:0809.3791](#)

Zimdahl, W., & Pavon, D. 2001, *Phys. Lett. B* **B521**, 133

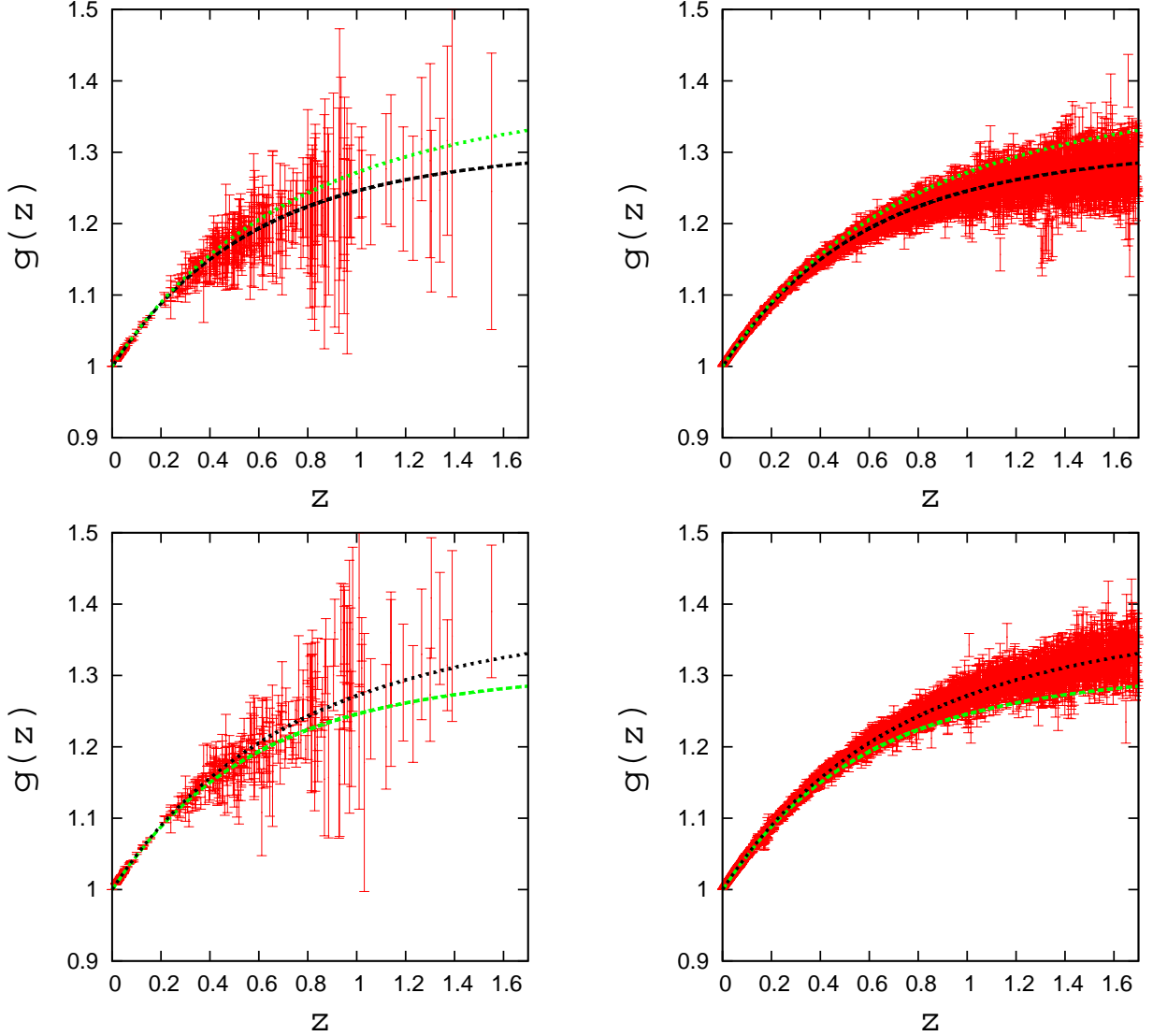


Fig. 1.— Reconstructed linear growth factor $g(z)$ for different datasets. The top panels show the results for Model 1 (Λ CDM) using Union-like (set A, left panel) and JDEM-like (set B, right panel) SNe datasets, while the bottom panels show results for Model 2 (variable w , eq (18)) using set A (left panel) and set B (right panel). In each figure, the black dotted line represents the true model, while the green dashed line represents the other model. The red solid lines show the 1σ error bars for the integral reconstruction using eq (12).

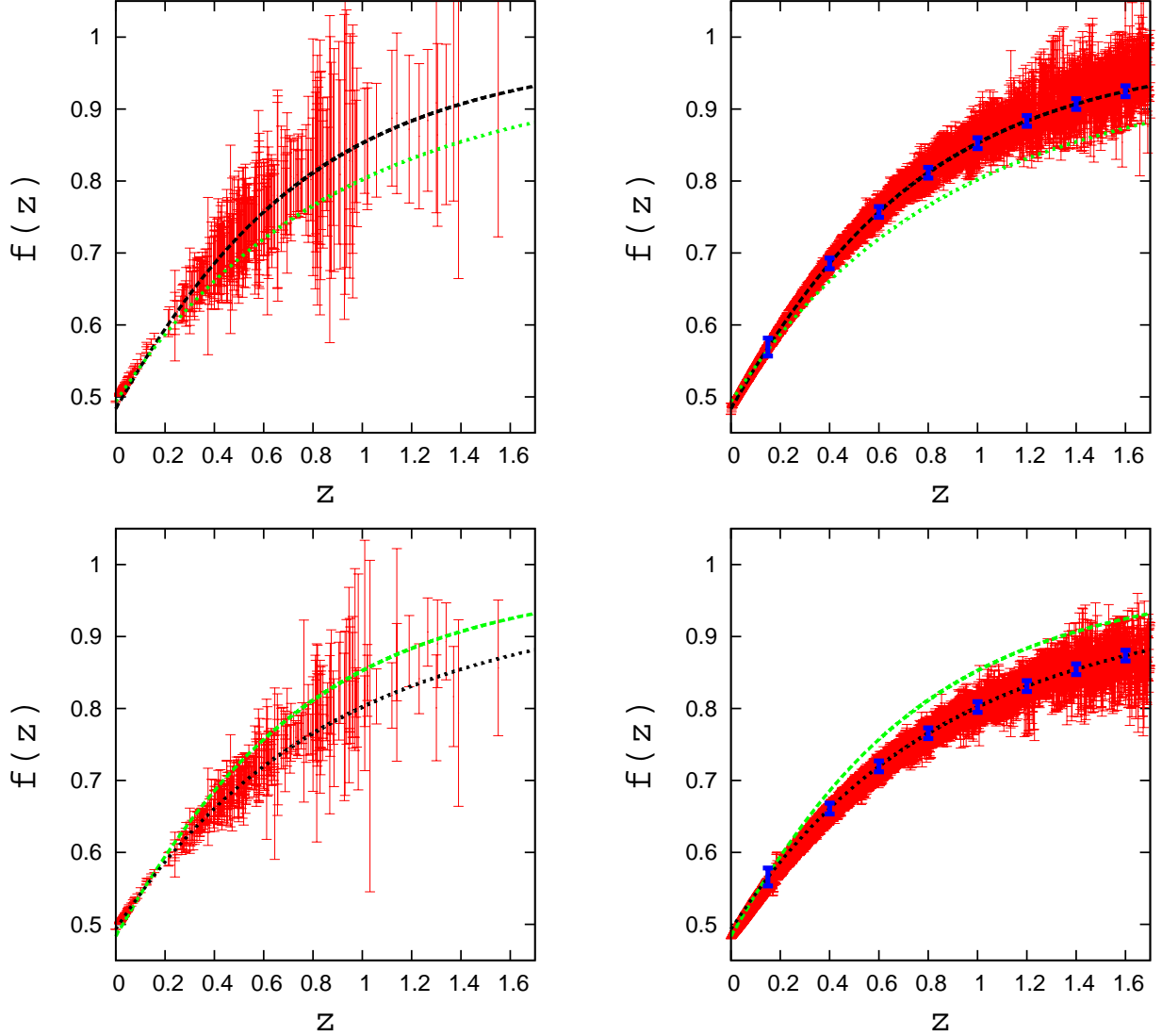


Fig. 2.— Reconstructed growth rate $f(z)$ for different datasets. The top panels show the results for Model 1 (Λ CDM) using Union-like (set A, left panel) and JDEM-like (set B, right panel) SNe datasets, while the bottom panels show results for Model 2 (variable w , eq (18)) using set A (left panel) and set B (right panel). In each figure, the thick black dotted line represents the true model, while the green dashed line represents the other model. The red solid lines show the 1σ error bars for the integral reconstruction using eq (12). The blue vertical lines in the right panel show the expected observational constraints from Euclid (Cimatti *et al.* 2008).

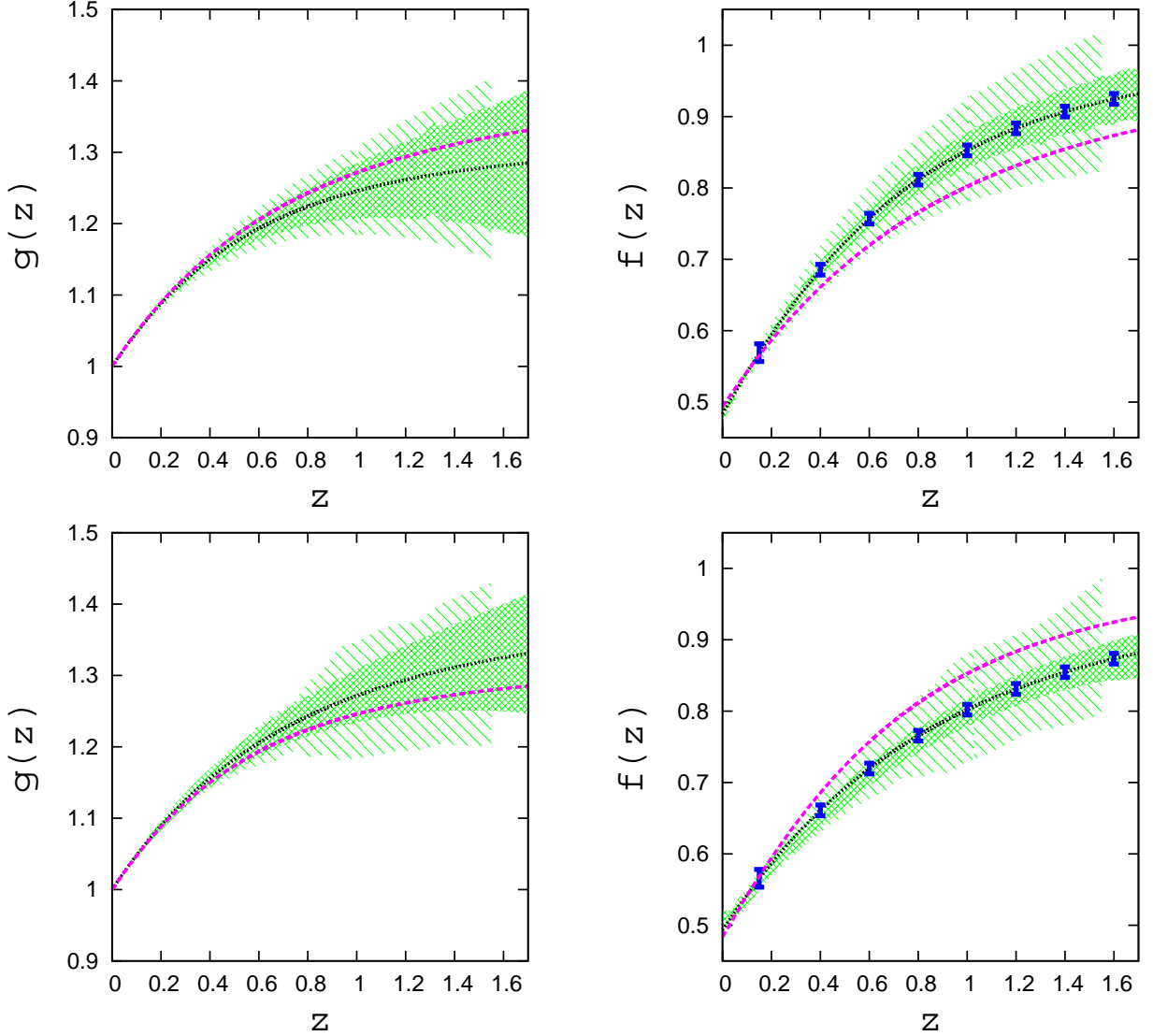


Fig. 3.— Reconstructed growth parameters for different datasets using the smoothing scheme Eq (16) on the integral reconstruction method, eq (12). The top panels show the results for Model 1 (Λ CDM) for the growth factor $g(z)$ (left panel) and the growth rate $f(z)$ (right panel). The bottom panels show the results for Model 2 (variable w , eq (18)) for $g(z)$ (left panel) and $f(z)$ (right panel). In each figure, the black dotted line represents the true model, while the pink dashed line represents the other model. The green dashed shaded area represents the 1σ errors for the integral reconstruction of set A (Union-like), while the green hatched shaded area represents the reconstruction for set B (JDEM-like). The blue vertical lines in the right panel show the expected observational constraints from Euclid (Cimatti *et al.* 2008).

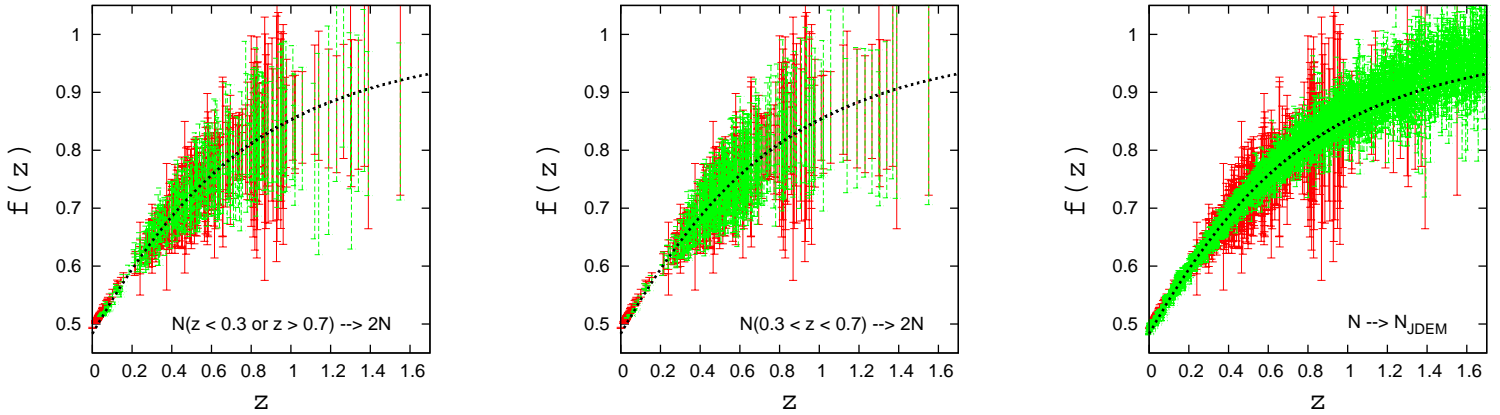


Fig. 4.— Reconstructed growth rate $f(z)$ for model 1 (Λ CDM) using various redshift distributions. We use (a) set A (Union-like) with number of SNe doubled at low and high redshifts (left panel) (b) set A with number of supernova doubled for mid-range SNe (center panel) and (c) JDEM-like (set B) redshift distribution with Union-like (set A) errors (right panel). In each panel, the red solid lines depict 1σ error bars on set A, while the green dashed lines show the 1σ error bars on set A modified according to (a), (b), (c). The black dotted line represents the true model.

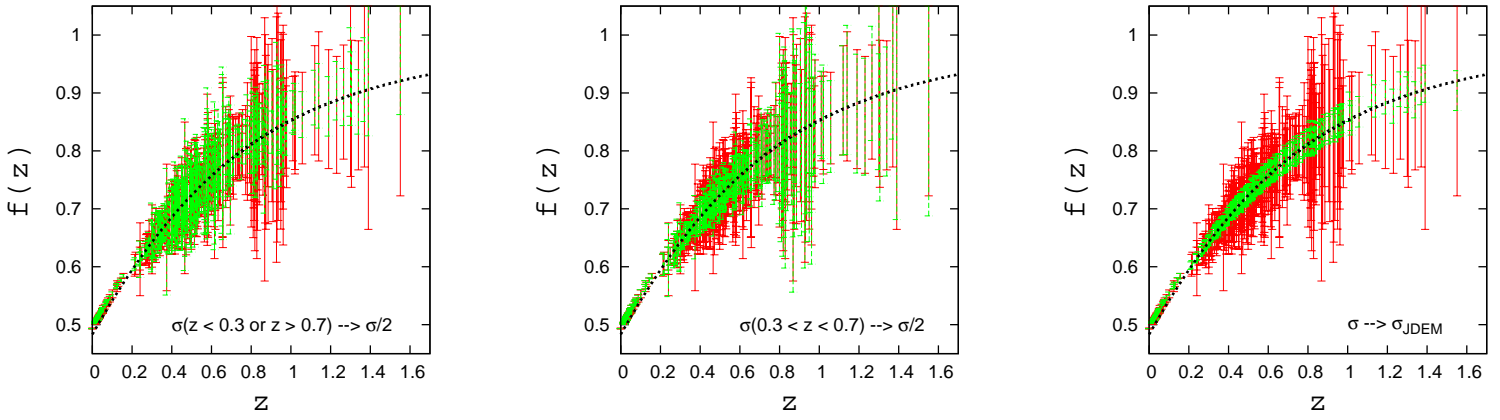


Fig. 5.— Reconstructed growth rate $f(z)$ for model 1 (Λ CDM) using various error distributions. We use (a) set A (Union-like) with errors halved at low and high redshifts (left panel) (b) set A with errors halved for mid-range SNe (center panel) and (c) set A with JDEM-like errors for each SNe (right panel). In each panel, the red solid lines depict 1σ error bars on set A, while the green dashed lines show the 1σ error bars on set A modified according to (a), (b), (c). The black dotted line represents the true model.

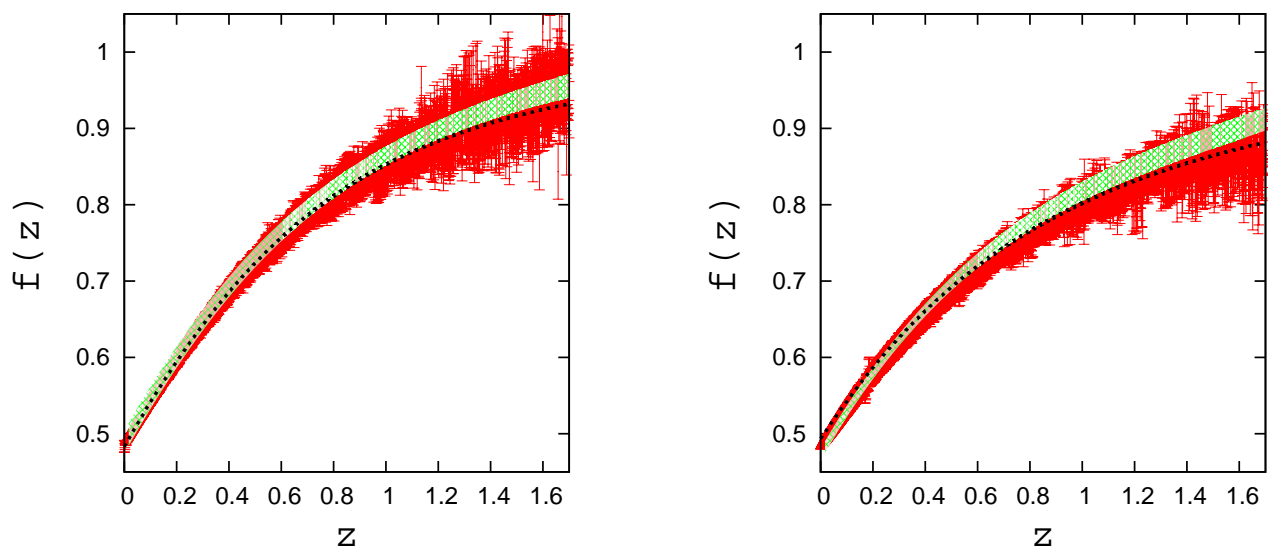


Fig. 6.— Reconstructed growth rate $f(z)$ for model 1 (left panel) and model 2 (right panel) using set B (JDEM-like) with different reconstruction methods. The red solid lines show the 1σ limits for reconstructed $f(z)$ using the integral reconstruction method, eq (12), while the green hatched region shows the 1σ limits for $f(z)$ using w parameterization, eqs (19), (21). The black dotted line represents the true model.

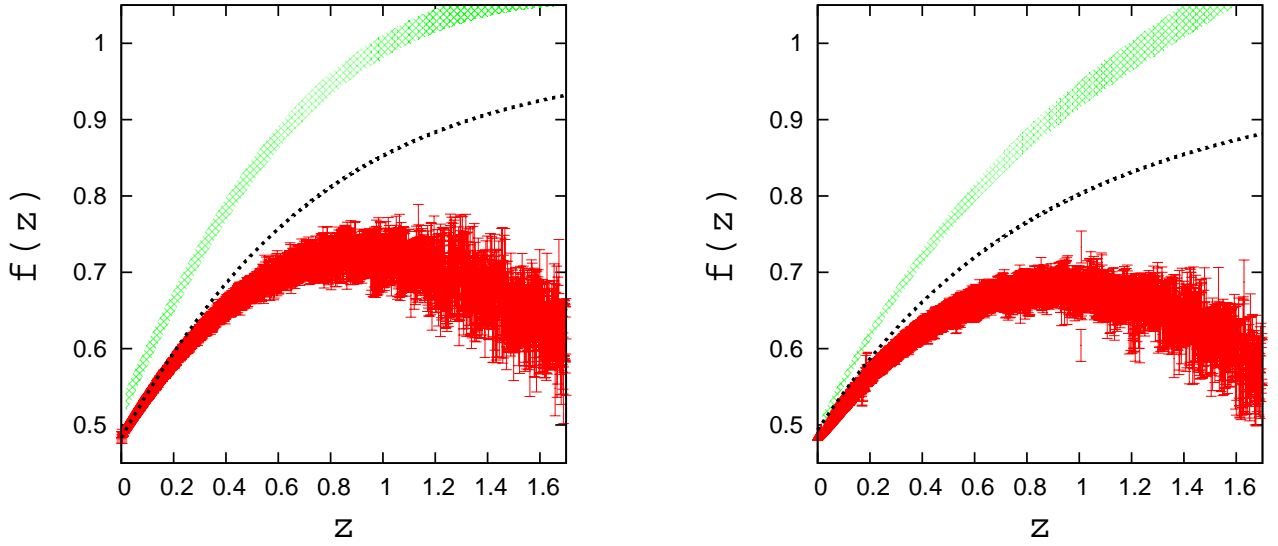


Fig. 7.— Reconstructed growth rate $f(z)$ for model 1 (left panel) and model 2 (right panel) for set B (JDEM-like) with different reconstruction methods, using $\Omega_{0m} = \Omega_{0m}(\text{true}) + 0.03$. The red solid lines show the 1σ limits for reconstructed $f(z)$ using the integral reconstruction method, eq (12), while the green hatched region shows the 1σ limits for $f(z)$ using w parameterization, eqs (19), (21). The black dotted line represents the true model. Note that the results for the two reconstructions lie on opposite sides of the true value of $f(z)$.

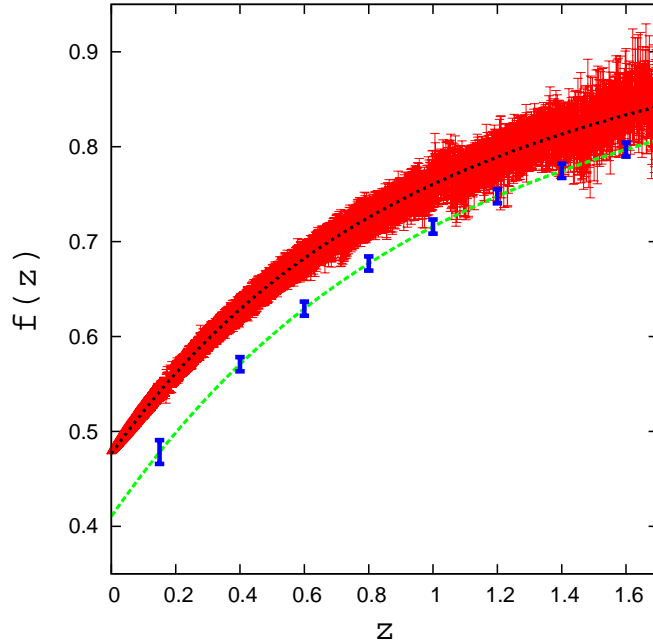


Fig. 8.— Reconstructed growth rate $f(z)$ for JDEM-like dataset using a modified gravity model (DGP, eq (23)). The thick black dotted line represents the result expected from just the expansion history (eq (19) using eq (23)), while the green dashed line represents the result expected from gravitational clustering (eq (24)). The red solid lines show the 1σ error bars for the integral reconstruction using eq (12). The blue vertical lines show the expected observational constraints from Euclid (Cimatti *et al.* 2008). The discrepancy between the two would act as a signal for modified gravity.

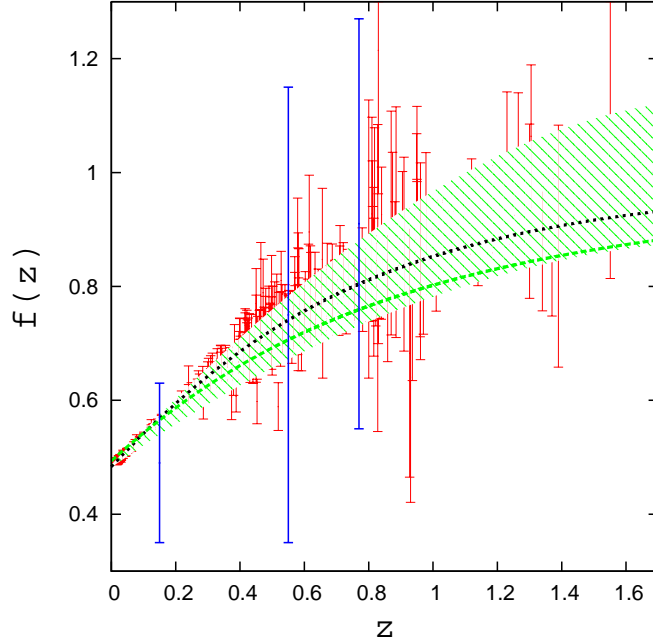


Fig. 9.— Reconstructed growth rate $f(z)$ for current Union set of SNe data, using $\Omega_{0m} = 0.26 \pm 0.03$. The red solid lines show the 1σ limits for reconstructed growth parameter using the integral reconstruction method, eq (12), while the green dashed shaded area shows the 1σ limits for the parameter using smoothing scheme, eq (16), for the integral reconstruction methods. The black dotted line shows $f(z)$ for LCDM, the green dashed line shows $f(z)$ for Model 2 (variable w , eq (18)). The three vertical blue lines show the current measurements of $f(z)$ from 2dFGRS (Verde *et al.* 2002), 2SLAQ (Ross *et al.* 2007) and VVDS (Guzzo 2008).

Table 1: Reconstructed linear growth factor g and growth rate f using different datasets for Model 1

Datasets	z	$g(z)$	$g_{\text{smooth}}(z)$	$g_{\text{exact}}(z)$	$f(z)$	$f_{\text{smooth}}(z)$	$f_{\text{exact}}(z)$
A (Union SNe)	0.3	1.11 ± 0.04	1.12 ± 0.02	1.12	0.65 ± 0.04	0.63 ± 0.03	0.64
	0.6	1.18 ± 0.05	1.18 ± 0.03	1.19	0.77 ± 0.06	0.75 ± 0.04	0.76
	1.0	1.27 ± 0.06	1.26 ± 0.05	1.25	0.82 ± 0.09	0.83 ± 0.06	0.85
	1.5	1.24 ± 0.15	1.26 ± 0.09	1.28	0.97 ± 0.21	0.94 ± 0.10	0.92
B (JDEM SNe)	0.3	1.13 ± 0.02	1.12 ± 0.01	1.12	0.64 ± 0.02	0.63 ± 0.01	0.64
	0.6	1.21 ± 0.03	1.20 ± 0.02	1.19	0.75 ± 0.04	0.76 ± 0.02	0.76
	1.0	1.24 ± 0.05	1.23 ± 0.03	1.25	0.86 ± 0.07	0.84 ± 0.03	0.85
	1.5	1.25 ± 0.08	1.26 ± 0.09	1.28	0.93 ± 0.11	0.92 ± 0.06	0.92
C (BOSS BAO)	2.5	1.28 ± 0.13	1.29 ± 0.11	1.30	1.01 ± 0.09	1.00 ± 0.07	0.97

Table 2: Reconstructed linear growth factor g and growth rate f using different datasets for Model 2

Datasets	z	$g(z)$	$g_{\text{smooth}}(z)$	$g_{\text{exact}}(z)$	$f(z)$	$f_{\text{smooth}}(z)$	$f_{\text{exact}}(z)$
A (Union SNe)	0.3	1.12 ± 0.03	1.12 ± 0.01	1.13	0.60 ± 0.04	0.61 ± 0.03	0.61
	0.6	1.20 ± 0.05	1.20 ± 0.03	1.21	0.70 ± 0.05	0.72 ± 0.05	0.72
	1.0	1.26 ± 0.07	1.27 ± 0.05	1.28	0.82 ± 0.09	0.81 ± 0.07	0.80
	1.5	1.34 ± 0.18	1.33 ± 0.10	1.32	0.89 ± 0.20	0.90 ± 0.13	0.87
B (JDEM SNe)	0.3	1.13 ± 0.02	1.11 ± 0.01	1.13	0.62 ± 0.02	0.61 ± 0.01	0.61
	0.6	1.19 ± 0.04	1.20 ± 0.02	1.21	0.71 ± 0.03	0.70 ± 0.02	0.72
	1.0	1.27 ± 0.05	1.27 ± 0.04	1.28	0.81 ± 0.04	0.80 ± 0.03	0.80
	1.5	1.33 ± 0.08	1.31 ± 0.07	1.32	0.88 ± 0.08	0.86 ± 0.04	0.87
C (BOSS BAO)	2.5	1.37 ± 0.13	1.35 ± 0.07	1.34	0.96 ± 0.11	0.94 ± 0.06	0.93

Table 3: Reconstructed linear growth factor g and growth rate f using current supernova data

z	$g(z)$	$g_{\text{smooth}}(z)$	$g_{\Lambda\text{CDM}}(z)$	$f(z)$	$f_{\text{smooth}}(z)$	$f_{\Lambda\text{CDM}}(z)$
0.3	1.13 ± 0.05	1.13 ± 0.05	1.12	0.62 ± 0.06	0.61 ± 0.04	0.64
0.6	1.21 ± 0.07	1.20 ± 0.06	1.19	0.79 ± 0.08	0.80 ± 0.05	0.76
1.0	1.29 ± 0.10	1.28 ± 0.07	1.25	0.93 ± 0.11	0.88 ± 0.08	0.85
1.5	1.37 ± 0.16	1.35 ± 0.12	1.28	1.05 ± 0.24	0.98 ± 0.11	0.92